Prediction of three-phase oil relative permeability through a sigmoid-based model

Ehsan Ranaee [a,*], Giovanni M. Porta [a], Monica Riva [a,b], Martin J. Blunt [a,c], Alberto Guadagnini [a,b]

[a] Dipartimento di Ingegneria Civile e Ambientale, Politecnico di Milano, Piazza L. Da Vinci 32, 20133 Milano, Italy
[b] Department of Hydrology and Water Resources, University of Arizona, Tucson, AZ 85721, USA
[c] Department of Earth Science and Engineering, Imperial College, London, SW7 2AZ, UK

Received 11 January 2014
Accepted 28 November 2014
Available online 6 December 2014

1. Introduction

Water alternating gas (WAG) injection techniques have been developed in recent years to increase oil recovery in mature reservoirs which have been exploited for several years. However, direct three-phase experimental data are often unavailable or incomplete. For this reason, relative permeability values in three-phase systems are typically obtained through interpolation models based on data col-lected under two-phase flow conditions. In this context, several empirical models have been proposed in the literature. A first set of models are based on the channel flow theory and assume that each pore is occupied by only one fluid (e.g., Stone, 1970, 1973; Aziz and Settari, 1979; Delshad and Pope, 1989). Baker (1988) introduced a second set of three-phase permeability models based on saturation-weighted interpolations of two-phase data. Along these lines, further developments are presented, e.g., by Jerauld (1997), Blunt (2000), DiCarlo et al. (2000), Egermann et al. (2000) and Shahverdi and Sohrabi (2012). Larsen and Skauge (1998) considered hysteresis effects due to gas phase trapping during WAG injection processes. Similar to two-phase hysteresis models (e.g., Killough, 1976; Carlson, 1981), their approach is grounded on the computation of the Land coefficient (Land, 1968).

Spiteri and Juanes (2006) compared the most commonly employed interpolation models against three-phase relative permeability data collected by Oak (1990). The authors show that (i) predictions based on channel flow theory are generally not accurate in reproducing three-phase oil relative permeability data, especially for low oil saturations, and (ii) the saturation weighted interpolation method proposed by Baker (1988) leads to severe underestimation of the observed oil relative permeability.

Here, we formulate two new empirical models and procedures to predict oil relative permeability during primary gas injection and secondary waterflooding, respectively. Our models are able to reproduce the effects of key physical processes which occur in a three-phase environment and are not included in currently available methods. In particular, they allow embedding within model predictions hysteresis effects and phase redistribution in the porous system. These features have been observed to play a relevant role during three-phase displacement (Van Dijke and Sorbie, 2003). We also propose a methodology for the estimation of the model parameters

* Corresponding author. Tel.: +39 223996285.
E-mail address: ehsan.ranaee@polimi.it (E. Ranaee).

Nomenclature

$\mathbf{C}_{kro}$ covariance matrix of oil relative permeability measurements error
k_{ro} three-phase oil relative permeability
k_{ro}^{G}, k_{ro}^{W} three-phase oil relative permeability for gas and water injection
k_{ro}^{J*} measured oil relative permeability in three-phase systems for gas ($I=G$) and water ($I=W$) injection
k_{ro}^{GS} sigmoid model for three-phase oil relative permeability following gas injection
k_{ro}^{inf} oil relative permeability at the inflection point of sigmoid model k_{ro}^{GS}
k_{row}^{inf} oil relative permeability at the inflection point of sigmoid model k_{row}^{S}
$\overline{k}_{rog}$ oil relative permeability in two-phase gas–oil systems
$\overline{k}_{row}^{i}, \overline{k}_{row}^{d}$ oil relative permeability in two-phase water–oil systems, respectively for imbibitions and drainage experiments
k_{row}^{S} sigmoid model for oil relative permeability in two-phase water–oil systems
$\overline{k}_{row}^{M}$ largest oil relative permeability in oil–water system
J objective function in ML model calibration
$\mathbf{J}$ sensitivity (Jacobian) matrix of oil relative permeability with respect to model parameters
m_{inf} first derivative of k_{ro}^{GS} at the inflection point
m_{og} slope observed for $\overline{k}_{rog}$ at the highest oil saturation value
S_g three-phase gas saturation
S_o three-phase oil saturation
$\overline{S}_{ow}^{M}$ maximum oil saturation in oil–water system
S_{oi} three-phase initial oil saturation
S_o^{inf} oil saturation at the inflection point of sigmoid model k_{ro}^{GS}
S_{ow}^{inf} oil saturation at the inflection point of sigmoid model k_{row}^{S}
S_w three-phase water saturation
$\overline{S}_{wc}, \overline{S}_{row}, \overline{S}_{gt}$ two-phase connate water, residual oil in oil–water system, and trapped gas saturations
$\mathbf{Q}$ covariance matrix of parameter estimates

Greek letters

λ, β parameters for the three-phase gas injection sigmoid model k_{ro}^{GS}
λ_{ow}, β_{ow} parameters for three-phase water injection sigmoid model k_{row}^{S}
$\overline{\lambda}, \overline{\beta}$ predicted values of sigmoid model parameters for three-phase primary gas injection systems based solely on two-phase observations
$\overline{\lambda}_{ow}, \overline{\beta}_{ow}$ predicted values of sigmoid model parameters for three-phase secondary water flooding systems based solely on two-phase observations
$\hat{\lambda}, \hat{\beta}, \hat{\lambda}_{ow}, \hat{\beta}_{ow}$ ML estimate of sigmoid model parameters
$\sigma_k, \hat{\sigma}_k$ standard deviation of measurement error and corresponding ML estimate
$\hat{\sigma}_{\lambda}, \hat{\sigma}_{\beta}$ ML estimates of standard deviation associated with $\hat{\lambda}, \hat{\beta}$
$\hat{\sigma}_{\lambda_{ow}}, \hat{\sigma}_{\beta_{ow}}$ ML estimates of standard deviation associated with $\hat{\lambda}_{ow}, \hat{\beta}_{ow}$

when (i) three-phase data are available or, as is typical of practical applications, (ii) when only two-phase data are accessible.

The paper is organized as follows. In Section 2 we introduce the sigmoid-based models for primary gas injection and secondary waterflooding, and discuss their ability to embed phenomenological issues observed in previous experiments. In Section 3 we describe the approaches proposed for calibration of model parameters on the basis of two-phase and/or three-phase data. Finally, in Section 4 we apply the proposed procedure to two sets of experimental data (Oak, 1990; Oak et al., 1990; DiCarlo et al., 2000). The robustness of the proposed methodology is assessed and demonstrated through comparison estimates of model parameter estimates relying solely on two-phase data against their counterparts estimated within a Maximum Likelihood (ML) framework (e.g., Carrera and Neuman, 1986; Riva et al., 2011 and references therein) on the basis of three-phase measurements. We test the proposed procedure by making use of the two- and three-phase data collected by Oak (1990) and the three-phase dataset of DiCarlo et al. (2000).

2. Model formulation

According to the saturation-weighted interpolation model (Baker, 1988), the oil relative permeability in a three-phase system, k_{ro}, can be evaluated as

$$k_{ro} = \frac{\left(S_w - \overline{S}_{wc}\right)\overline{k}_{row}^{i} + \left(S_g - \overline{S}_{gt}\right)\overline{k}_{rog}}{\left(S_w - \overline{S}_{wc}\right) + \left(S_g - \overline{S}_{gt}\right)} \tag{1}$$

Here, k_{row}^{S} and $\overline{k}_{rog}$ respectively are water and gas saturations for three-phase flow conditions; $\overline{S}_{wc}$ and $\overline{k}_{rog}$ respectively are connate water saturation and oil relative permeability in an oil–gas environment; $\overline{S}_{gt}$ is the trapped gas saturation, i.e. $\overline{S}_{gt}$ is the lowest gas saturation observed in oil–gas experiments at the end of oil injection; $\overline{k}_{row}^{i}$ is the oil relative permeability in oil–water environment when water is injected (corresponding to an imbibition process in a water-wet system). Note that here and in the following all saturations and permeabilities indicated with an overbar ($\bar{\cdot}$) are associated with two-phase systems. As recalled in Section 1, equation (1) does not properly predict observed oil relative perme-ability values (Spiteri and Juanes, 2006).

In the following we introduce two new models to predict oil relative permeabilities in three-phase environments during primary gas injection (Section 2.1) and secondary water injection (Section 2.2).

2.1. Modeling primary gas injection

We propose the following model to predict three-phase oil relative permeability during primary gas injection, k_{ro}^{G}

$$k_{ro}^{G} = \max(k_{ro}^{GS}, \overline{k}_{rog}) \quad \text{with } k_{ro}^{GS} = \frac{\overline{k}_{row}^{M} S_o}{\overline{S}_{ow}^{M} + \exp\left[\lambda - \beta (S_o / \overline{S}_{ow}^{M})^{\overline{S}_{ow}^{M}}\right]} \tag{2}$$

Here, S_o is the oil saturation in the three-phase system, λ and β are model parameters, $\overline{S}_{ow}^{M}$ and $\overline{k}_{row}^{M}$ respectively are the largest oil saturation and relative permeability observed in a two-phase oil–water system. This equation is consistent with previous experimental findings (e.g., DiCarlo et al., 2000) and empirical interpretive models (e.g., Blunt, 2000) highlighting that three-phase oil relative permeability values at low oil saturations are relatively close to $\overline{k}_{rog}$. Eq. (2) introduces a sigmoid function whose model parameters,

λ and β, are linked to the coordinates $(S_o^{inf}, k_{ro}^{inf})$ of the inflection point of k_{ro}^{GS} and to the derivative of k_{ro}^{GS} with respect to S_o at the inflection point, m_{inf} (i.e., to the slope of the tangent to k_{ro}^{GS} at the inflection point) by

$$\lambda = \ln\left[\frac{\bar{k}_{row}^{M} S_o^{inf}}{k_{ro}^{inf}} - \bar{S}_{ow}^{M}\right] + \beta \left(\frac{S_o^{inf}}{\bar{S}_{ow}^{M}}\right)^{\bar{S}_{ow}^{M}} \tag{3}$$

$$\beta = \frac{1}{\bar{S}_{ow}^{M}} \left(\frac{m_{inf} S_o^{inf}}{k_{ro}^{inf}} - 1\right) \left(1 - \frac{\bar{S}_{ow}^{M} k_{ro}^{inf}}{\bar{k}_{row}^{M} S_o^{inf}}\right)^{-1} \left(\frac{S_o^{inf}}{\bar{S}_{ow}^{M}}\right)^{-\bar{S}_{ow}^{M}} \tag{4}$$

Fig. 1 depicts the dependence of k_{ro}^{GS} on S_o as a function of (i) λ for $\beta = 27.24$ (Fig. 1a) and (ii) β for $\lambda = 15.68$ (Fig. 1b) upon setting $\bar{k}_{row}^{M} = 0.89$ and $\bar{S}_{ow}^{M} = 0.74$. The values adopted for the fixed parameters in the plots correspond to those associated with the two-phase experimental data of Oak (1990) which we employ in our analyses, as detailed in Section 4. It can be noted that the two parameters λ and β have a different influence on the k_{ro}^{GS} behavior. An increase of λ causes k_{ro}^{GS} to decrease. When $\lambda \to \infty$, k_{ro}^{GS} vanishes for all oil saturation values. At intermediate oil saturation values (i.e., $0.2 < S_o < 0.5$) the rate of increase of k_{ro}^{GS} with S_o effectively displays only minute variability with λ for all practical purposes. On the other hand, this rate is strongly affected by β (see Fig. 1b). For large β values, k_{ro}^{GS} is observed to sharply increase with S_o for low saturations. This suggests that β might imbue effects associated with oil displacement at low S_o values. This aspect is investigated in Section 3.

2.2. Modeling secondary water injection

As suggested by the results of Spiteri and Juanes (2006), hysteretic effects on oil relative permeabilities in three-phase flow during secondary water injection, k_{ro}^{W}, can be neglected. Therefore, we propose the following model to represent this scenario:

$$k_{ro}^{W} = \frac{\left(S_w - \bar{S}_{wc}\right) k_{row}^{S} + \left(S_g - \bar{S}_{gt}\right) \bar{k}_{rog}}{\left(S_w - \bar{S}_{wc}\right) + \left(S_g - \bar{S}_{gt}\right)}$$

$$\text{with } k_{row}^{S} = \frac{\bar{k}_{row}^{M} \bar{S}_{ow}}{\bar{S}_{ow}^{M} + \exp\left[\lambda_{ow} - \beta_{ow} (\bar{S}_{ow}/\bar{S}_{ow}^{M})^{\bar{S}_{ow}^{M}}\right]} \tag{5}$$

Here, $\bar{S}_{ow}$ is oil saturation in an oil–water environment, all the remaining quantities being defined above. The modeling choice upon which (5) relies corresponds to the commonly adopted saturation-weighted interpolation scheme (1), where $\bar{k}_{row}^{i}$ is replaced by the sigmoid-curve k_{row}^{S} to include the effects of pore-scale changes of fluids arrangement as a function of the relative amount of water and gas in the system. The sigmoid parameters, λ_{ow} and β_{ow}, are linked to the characteristics of the inflection point of k_{row}^{S} by relationships analogous to (3)–(4). The phenomenological rationale underlying (2) and (5) is discussed in Section 2.3.

2.3. The phenomenological picture

The model formulations presented in Sections 2.1 and 2.2 are here discussed in light of experimental data and their physical interpretation.

The classical saturation-weighted interpolation model (1) indicates that k_{ro} should be fall between $\bar{k}_{row}^{i}$ and $\bar{k}_{rog}$ for all oil saturation values. This is often not supported by experimental evidence, as shown for example in Fig. 2, where experimental three-phase oil relative permeabilities measured by Oak (1990) during primary gas injection, k_{ro}^{G}, and secondary water flooding, k_{ro}^{W}, clearly lie outside the region delimited by $\bar{k}_{row}^{i}$ and $\bar{k}_{rog}$. In particular, it can be noted that k_{ro}^{G} and k_{ro}^{W} are generally larger than $\bar{k}_{row}^{i}$ and $\bar{k}_{rog}$.

The inaccuracy of predictions of k_{ro} based on (1) suggests that the occurrence of a third phase in the porous system has a strong impact on the functional format of the relationship between oil relative permeability and oil saturation (Ranaee et al., 2014). As a result, it is not possible to reproduce observed three-phase relative permeabilities by means of models based on simple linear interpolation of two-phase data. This observation is also consistent with pore network modeling results documenting complex features associated with three-phase flow conditions (e.g., Van Dijke and Sorbie, 2003; Van

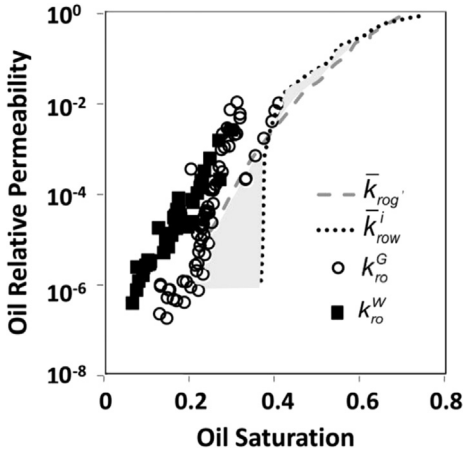

Fig. 2. Measured oil relative permeabilities (symbols) under two-phase (oil–water, $\bar{k}_{row}^{i}$, oil–gas, $\bar{k}_{rog}$) and three-phase (k_{ro}^{G}, k_{ro}^{W}) conditions. The shaded area indicates the region where predictions provided by (1) are comprised. Data are from Oak (1990).

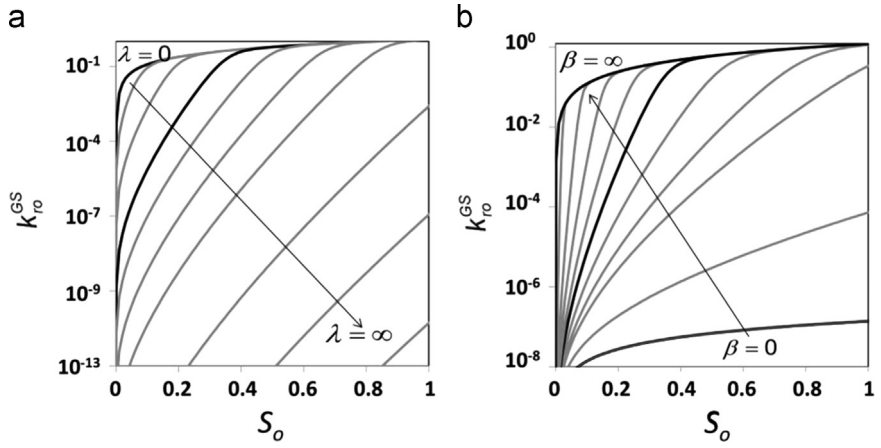

Fig. 1. Dependence of k_{ro}^{GS} on S_o for different values of (a) λ for $\beta = 27.24$ and (b) β for fixed $\lambda = 15.68$ ($\bar{k}_{row}^{M} = 0.89$ and $\bar{S}_{ow}^{M} = 0.74$ for all cases).

Dijke et al., 2006; Piri and Blunt, 2005; Suicmez et al., 2007, 2008) and/or visualization of experiments in micromodel studies (e.g., Sohrabi et al., 2008).

The sigmoid-based approach formulated in (2)–(5) incorporates diverse physical peculiarities characterizing three-phase flow into a unique predictive model.

During WAG procedures the primary gas injection starts at the end of the primary waterflooding, i.e., at residual oil saturation, $S_{oi} = \overline{S}_{row}$, where $\overline{k}^{i}_{row} \approx 0$, as indicated in Fig. 3a. If the rock is water-wet, water occupies the smallest pores whereas oil resides in the largest pores. It has been shown (e.g., Van Dijke and Sorbie, 2003) that injection of gas tends to move the oil from the largest to the smallest pores. Previous studies in water-wet systems (Blunt, 2000; DiCarlo et al., 2000; Fenwick and Blunt, 1998) show that for low saturations oil tends to flow in layers between water (which flows in contact with the solid matrix) and gas (which occupies the central part of the void space). Experimental measurements (Alizadeh and Piri, 2013, 2014) and pore network numerical results (e.g., Mani and Mohanty, 1997) show that formation of oil layers plays an important role in three-phase flow for positive values of the spreading coefficient. As a consequence of the formation of oil layers, residual oil (from primary waterflooding) is then remobilized during primary gas injection and the oil relative permeability tends to increase. Under these conditions, the simple relationship $k^{G}_{ro} \propto {S_o}^2$ holds for low oil saturations (Fenwick and Blunt, 1998; DiCarlo et al., 2000). This ultimately leads to very low values of residual oil saturations (Blunt, 2000). Our sigmoid-based model embeds the occurrence of a smooth transition from oil remobilization, as induced by gas injection, towards the spreading layer drainage regime. Note, however, that the oil relative permeability typically reaches very small values at low oil saturations, meaning that recovery becomes very slow.

As previously noticed, model (5) proposed for secondary water injection is based on the saturation-weighted interpolation method (1), where $\overline{k}^{i}_{row}$ is replaced by the sigmoid function k^{S}_{row}. As a consequence, this enables us to account for the reduction of residual oil saturation in a three-phase system, as compared to oil–water (two-phase) environments. Our model implies that $k^{S}_{row} = 0$ when $\overline{S}_{ow} = 0$, i.e., no residual oil saturation is assumed to occur for secondary waterflooding. With respect to this point, we note that the secondary waterflooding data which are described in Section 4.2 include a significant amount of gas ($S_g > 0.3$) and are therefore not suited to the characterization of oil trapping.

3. Estimation of model parameters

Sigmoid models (2) and (5) require the calibration of two parameters, i.e., (λ, β) and $(\lambda_{ow}, \beta_{ow})$ respectively. In Section 3.1 we detail a methodology to estimate these parameters when only two-phase relative permeability data are available. Then, in Section 3.2 we introduce a Maximum Likelihood (ML) framework which can be employed to calibrate model parameters in the presence of three-phase observations of oil relative permeabilities.

3.1. Parameter estimation through two-phase data only

In the following we detail two procedures to compute (λ, β) (see Section 3.1.1) and $(\lambda_{ow}, \beta_{ow})$ (see Section 3.1.2), when only two-phase data are available, as is typically the case in practical applications. The procedure requires the knowledge of two types of datasets: (a) oil relative permeabilities measured during drainage (oil injection), $\overline{k}^{d}_{row}$, and imbibition, $\overline{k}^{i}_{row}$ in a water–oil system (see, for example, Fig. 3a) and (b) oil relative permeabilities obtained during gas injection into a porous medium saturated with oil in the presence of connate water, $\overline{k}_{rog}$ (see, for example, Fig. 3b).

3.1.1. Primary gas injection

Our modeling strategy relies on the assessment of the inflection point $(S^{inf}_{o}, k^{inf}_{ro})$, of k^{GS}_{ro}, and m_{inf} introduced in (3)–(4) according to the following procedure, which is graphically exemplified in Fig. 3.

(1) We assume that the location of the inflection point of k^{GS}_{ro} is identified by the beginning of gas injection, corresponding to $S^{inf}_{o} = S_{oi}$. We also set $k^{GS}_{ro} = \overline{k}^{d}_{row}(S_{oi})$, i.e., k^{inf}_{ro} coincides with the relative permeability observed during drainage in an oil–water system at saturation, $S^{inf}_{o} = S_{oi}$ (see Fig. 3a). This hypothesis simulates the remobilization of oil due to the injection of gas described in the previous section and is consistent with the hysteresis model of Carlson (1981). Consequently, our model implicitly assumes that the efficiency of oil remobilization is a function of the initial oil saturation.

(2) We set the slope, m_{inf}, of k^{GS}_{ro} at the inflection point $(S^{inf}_{o}, k^{inf}_{ro})$ to the value observed in the two-phase gas–oil system at the highest oil saturation. In other words, we assume that $m_{inf} = m_{og}$, m_{og} being the slope observed for $\overline{k}_{rog}$ at the highest S_o value, as exemplified in Fig. 3b. This hypothesis is justified by the observation that the largest rate of change of oil relative permeability with S_o occurs at the beginning of the gas injection.

Substitution of $S^{inf}_{o} = S_{oi}$, $k^{inf}_{ro} = \overline{k}^{d}_{row}(S_{oi})$ and $m_{inf} = m_{og}$ into (3)–(4) provides an estimate of (λ, β) solely on the basis of two-phase observations. We label such estimates as $(\overline{\lambda}, \overline{\beta})$ in the following. A graphical representation of the resulting prediction curve for k^{GS}_{ro} is provided in Fig. 3c (solid curve).

In summary, the method we propose allows estimating three-phase oil relative permeability for primary gas injection on the

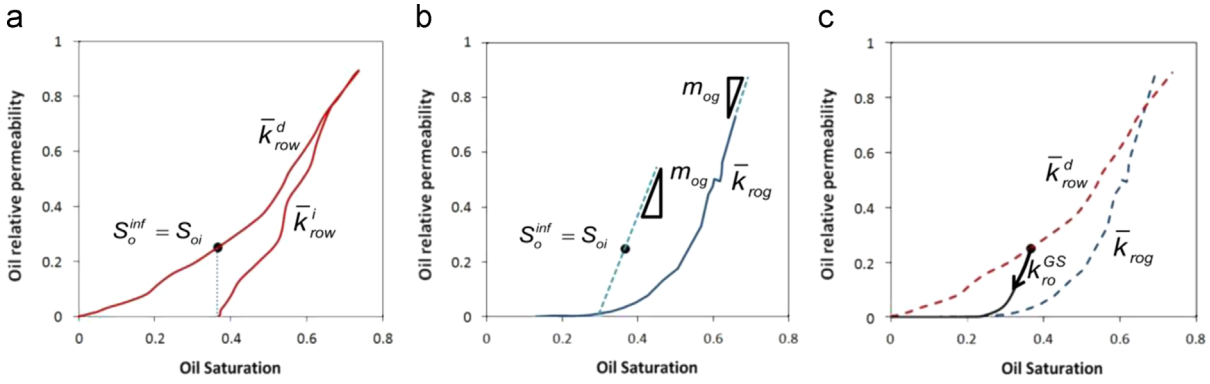

Fig. 3. Key steps exemplifying the estimation of k^{GS}_{ro} based on two-phase oil relative permeability data: (a) positioning of the inflection point along $\overline{k}^{d}_{row}$; (b) definition of m_{inf}; and (c) final sigmoid model (solid curve). The procedure leads to prediction of k^{GS}_{ro} for $S_o < S^{inf}_{o}$ as indicated by the direction of the arrow in (c).

basis of the following information: (i) the initial oil saturation observed at the onset of gas injection; (ii) two-phase oil–water drainage data; and (iii) the rate of change of relative permeability at the largest oil saturation observed in the two-phase oil–gas environment. Note that (in principle) one might consider using our methodology in conjunction with Corey-type approximations (Corey and Rathjens, 1956) to (a) represent two-phase relative permeabilities in the absence of two-phase data or (b) smooth out perturbations induced by measurement errors associated with two-phase data.

3.1.2. Secondary water injection

We employ the following procedure, which is graphically exemplified in Fig. 4. We assume that the inflection point $(S_{ow}^{inf}, k_{row}^{inf})$ of k_{row}^{S} lies on the curve $\overline{k}_{row}^{i}$, i.e., $k_{row}^{inf} = \overline{k}_{row}^{i}(S_{ow}^{inf})$, and set S_{ow}^{inf} as the average saturation between $\overline{S}_{row}$ and $\overline{S}_{ow}^{M}$ (see also Fig. 4a) i.e.,

$$S_{ow}^{inf} = \overline{S}_{row} + \frac{\overline{S}_{ow}^{M} - \overline{S}_{row}}{2} \tag{6}$$

The slope, m_{ow}^{inf}, of k_{row}^{S} at the inflection point is estimated as (see Fig. 4a)

$$m_{ow}^{inf} = \frac{k_{row}^{inf}}{S_{ow}^{inf} - \overline{S}_{row}} \tag{7}$$

These hypotheses are validated in Section 4.12.

Substitution of (6) and (7) into (3)–(4) (after replacing λ by λ_{ow}, S_o^{inf} by S_{ow}^{inf}, β by β_{ow} and k_{ro}^{inf} by k_{row}^{inf}) provides the estimate of $(\lambda_{ow}, \beta_{ow})$ solely on the basis of only two-phase observations. We label such estimates as $(\overline{\lambda}_{ow}, \overline{\beta}_{ow})$ in the following. A graphical representation of the resulting prediction curve for k_{row}^{S} is provided in Fig. 4c. Note that k_{row}^{S} in Fig. 4c is qualitatively similar to the waterflood curve in a water–oil system $\overline{k}_{row}^{i}$ for large oil saturation $(S_{ow} > \overline{S}_{row})$ and smoothly approaches zero for $S_o \to 0$. The predicted values for the three-phase relative permeability k_{ro}^{W} are then obtained by (5), i.e., through saturation-weighted interpolation of the curves k_{row}^{S} and $\overline{k}_{rog}$, as illustrated in Fig. 4c.

3.2. Parameter calibration using three-phase data

We also perform calibration of the parameters embedded in the models described in Section 2 when three-phase relative permeability data are available. The procedure is grounded within the Maximum Likelihood (ML) framework and ML estimates, $(\hat{\lambda}, \hat{\beta})$ and $(\hat{\lambda}_{ow}, \hat{\beta}_{ow})$, of model parameters, (λ, β) and $(\lambda_{ow}, \beta_{ow})$, are obtained by minimizing the negative log likelihood criterion (e.g., Carrera and Neuman, 1986; Medina and Carrera, 2003)

$$NLL = \frac{J}{\sigma_k^2} + N \ln \sigma_k^2 + N \ln(2\pi) \tag{8}$$

Here J is the global residual between model predictions and observations defined as:

$$J = \sum_{j=1}^{N} \left[\log k_{ro,j}^{I}(S_o) - \log k_{ro,j}^{I*}(S_o) \right]^2 \text{ with } I = G, W \tag{9}$$

where N is the number of three-phase oil relative permeability data, $k_{ro,j}^{I*}(S_o)$, available during primary gas injection (when $I=G$) or secondary water injection (when $I=W$), $k_{ro,j}^{I}$ are the corresponding model predicted values obtained by (2) (when $I=G$) or by (5) (when $I=W$). In (9) we assume that the covariance matrix of the oil permeability measurements error, $\mathbf{C}_{kro}$, can be written as $\mathbf{C}_{kro} = \sigma_k^2 \mathbf{I}$, where $\mathbf{I}$ is the identity matrix and σ_k^2 is measurement error variance. A ML estimate of σ_k^2 can be obtained as $\hat{\sigma}_k^2 = J_{min}/N$, where J_{min} is the minimum value of J as a result of optimization (e.g., Carrera and Neuman, 1986; Riva et al., 2011 and references therein).

The uncertainty associated with parameter estimates is evaluated through a Cramer-Rao lower-bound approximation of the parameter estimation covariance matrix, $\mathbf{Q}$, (e.g., Riva et al., 2009), i.e.:

$$\mathbf{Q} = \sigma_k^2 \left(\mathbf{J}^T \mathbf{J} \right)^{-1} \tag{10}$$

Here, $\mathbf{J}$ is the Jacobian (sensitivity) matrix of relative permeabilities derivatives with respect to model parameters evaluated at $(\hat{\lambda}, \hat{\beta})$ when $I=G$ or $(\hat{\lambda}_{ow}, \hat{\beta}_{ow})$ when $I=W$. The diagonal elements of $\mathbf{Q}$ provide lower bound estimates of the parameter estimation variances, $\hat{\sigma}_{\lambda}^2$ and $\hat{\sigma}_{\beta}^2$. Various numerical methodologies can be adopted for the minimization of (8) or, equivalently, of (9). Here, we employ three methods, the imperialist competitive algorithm (ICA) (Atashpaz-Gargari and Lucas, 2007), the global pattern search (GPS) (Wetter and Wright, 2003), and the gradient method (GM) (Doherty, 2005; Nocedal and Wright, 2006), to explore the robustness of the resulting parameter estimates. Implementation of the three algorithms has been performed in the Matlab® environment. All three methodologies lead to almost undistinguishable results (details not reported). In the following we report only the key results obtained via the ICA.

4. Application to experimental results and model validation

In this section we apply and validate the methodology developed in Sections 2 and 3 to two available datasets, respectively presented by Oak (1990) (Section 4.1) and DiCarlo et al. (2000) (Section 4.2). The two data sets differ in terms of (i) properties of the host porous media and (ii) physical processes involved and

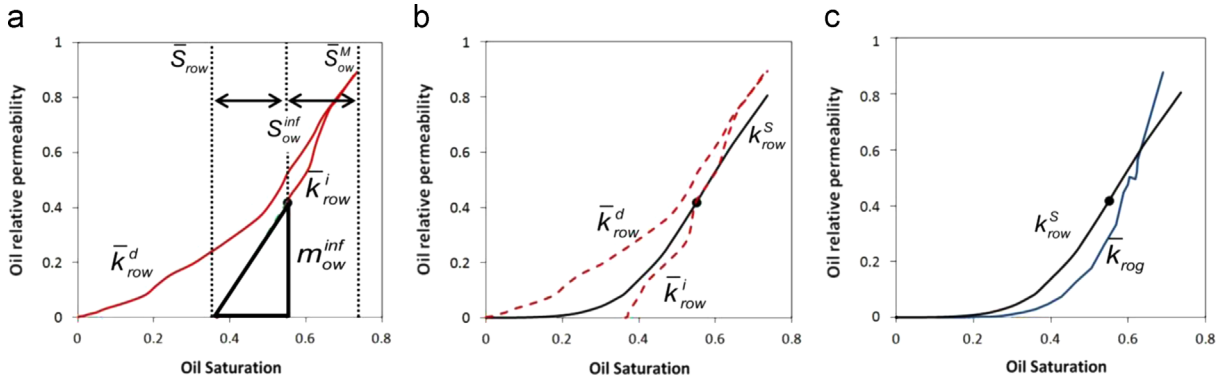

Fig. 4. Key steps of the procedure for the estimation of k_{row}^{S} based on two-phase oil relative permeability data: (a) positioning the inflection point along $\overline{k}_{row}^{i}$ and definition of m_{ow}^{inf}; (b) constructed sigmoid model k_{row}^{S}; and (c) comparison between k_{row}^{S} and $\overline{k}_{rog}$. The final estimated values of the three-phase relative permeability k_{ro}^{W} are obtained through saturation-weighted interpolation of k_{row}^{S} and $\overline{k}_{rog}$.

allow validating our sigmoid-based models as well as our parameter estimation procedure for a broad range of practical and realistic settings.

4.1. Analysis of the experiments of Oak (1990)

The Oak dataset comprises a series of two-phase (oil–water and oil–gas) and three-phase oil relative permeabilities measured on three sandstone core samples under steady-state conditions. Among these, we select those related to a water-wet Berea core (labeled core #6 in Oak, 1990) that include a complete set of two- and three-phase measurements required for the purpose of our analysis (Oliveira and Demond, 2003). Estimates obtained through the models proposed in Section 2 are here compared against the experimental observations documented by Oak (1990). Results for primary gas injection (Section 4.1.1) and secondary water injection (Section 4.1.2) are presented and discussed.

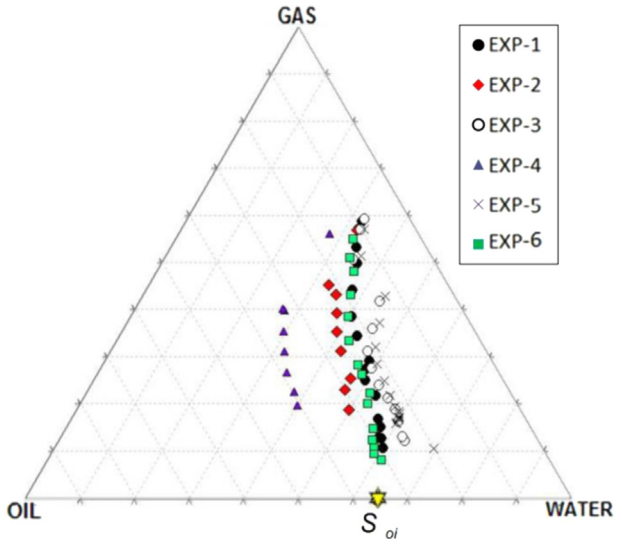

Fig. 5. Saturation paths of the primary gas injection experiments considered. Data are from Oak (1990). The yellow triangle on the oil–water side indicates the waterflood residual oil saturation which is here assumed to be the starting point for the gas injection experiments.

Table 1
Coordinates (S_o^{inf}, k_{ro}^{inf}) of the inflection point of the sigmoid model (2), largest values of oil saturation, $\overline{S}_{ow}^{M}$, and associated relative permeability, $\overline{k}_{row}^{M}$, in the oil–water system, m_{inf} and estimates ($\overline{\lambda}$, $\overline{\beta}$) derived from primary gas injection experiments reported by Oak (1990).

S_o^{inf}	k_{ro}^{inf}	$\overline{S}_{ow}^{M}$	$\overline{k}_{row}^{M}$	m_{inf}	$\overline{\lambda}$	$\overline{\beta}$
0.36	0.25	0.74	0.89	4.24	15.68	27.23

4.1.1. Primary gas injection

We consider a set of six primary gas injection three-phase experiments performed by Oak (1990). The saturation paths of the six experiments are depicted in Fig. 5. First we present the results obtained by estimating the model parameters using only two-phase data, as described in Section 3.1. The outcomes of this analysis are then compared with those yielded by ML calibration of model parameters described in Section 3.2.

As described in Section 3.1, we assume for all experiments the initial oil saturation to be equal to the residual oil saturation in an oil–water system after imbibition, S_{oi} (see Fig. 5). This choice is related to our assumption that gas injection starts at the end of waterflooding.

Table 1 lists the values of $S_{oi} = S_o^{inf}$ and $\overline{k}_{row}^{d}(S_{oi}) = k_{ro}^{inf}$, the largest values of oil saturation, $\overline{S}_{ow}^{M}$, and the associated relative permeability, $\overline{k}_{row}^{M}$, in the oil–water system together with the maximum slope ($m_{inf} = m_{og}$) of the oil permeability curve in the oil–gas system. Parameter estimates ($\overline{\lambda}, \overline{\beta}$) obtained as described in Section 3.1.1 are also listed. Fig. 6a depicts the scatterplot of predicted versus observed oil relative permeability values. Predictions are generally accurate, although it can be seen that our model significantly overestimates the data collected in Experiment 4. However, from Fig. 5 we note that several oil saturation values observed during Experiment 4 are larger than S_{oi}. Therefore, the inability of our model to reproduce the outcomes of Experiment 4 can be attributed to the observation that gas injection in this experiment started at an (unknown) oil saturation value which is presumably larger than the residual oil saturation at the end of waterflooding.

We then applied the ML procedure described in Section 3.2 to obtain ML estimates of (λ, β) using three-phase oil permeability data as well as the values of $\overline{S}_{ow}^{M}$ and $\overline{S}_{row}^{M}$ listed in Table 1. Table 2 lists ML estimates ($\hat{\lambda}, \hat{\beta}$) together with the corresponding estimation error variance (i.e., $\hat{\sigma}_{\lambda}$ and $\hat{\sigma}_{\beta}$) evaluated by considering each experiment individually as well as by analyzing jointly all experiments while excluding Experiment 4. Fig. 6b depicts a scatterplot of predicted and observed oil relative permeability values. The ML

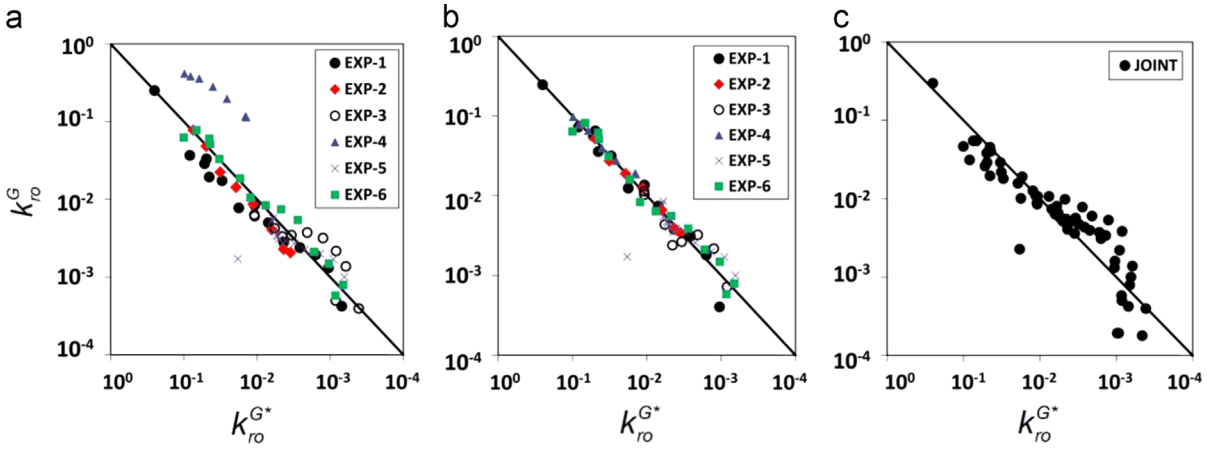

Fig. 6. Scatterplots of observed (k_{ro}^{G*}) and predicted (k_{ro}^{G}) three-phase oil relative permeability values following gas injection. Model predictions are obtained with (a) ($\overline{\lambda}, \overline{\beta}$) listed in Table 1; (b) ($\hat{\lambda}, \hat{\beta}$) listed in Table 2 and calibrated considering each experiment independently; and (c) ($\hat{\lambda}, \hat{\beta}$) listed in Table 2 and calibrated considering jointly all the experiments.

calibrated model always leads to highly accurate predictions of three-phase oil relative permeabilities, demonstrating the robustness of our proposed sigmoid-based model. Making use of (3) and (4), estimates of $\hat{\lambda}$ and $\hat{\beta}$ can then be related *a posteriori* to the coordinates (S_o^{inf}, k_{ro}^{inf}) of the inflection point and to m_{inf}. These latter values are also listed in Table 2 for completeness. These results indicate that the estimated initial oil saturation associated with Experiment 4 is significantly larger than the residual oil saturation listed in Table 1 and than the corresponding values predicted by the remaining experiments. This observation supports our conjecture that Experiment 4 started at an oil saturation level larger than S_{oi}.

Fig. 6c depicts the scatterplot of observed and predicted relative permeability values obtained on the basis of the ML model calibration procedure applied by considering jointly all available data, while excluding Experiment 4 for the reasons illustrated above. It can be noted that this plot is virtually undistinguishable from Fig. 6a, proving further support to the ability of our suggested procedure to properly estimate the model parameters only on the basis of two-phase data.

Table 2

Number of available three-phase relative permeability data (N), ML estimates $(\hat{\lambda}, \hat{\beta})$ and corresponding estimation error standard deviations, m_{inf}, coordinates (S_o^{inf}, k_{ro}^{inf}) of the inflection point of (2) and ML estimate of the variance $\hat{\sigma}_k^2$ of three-phase oil permeability measurement errors derived for each primary gas injection experiment reported by Oak (1990).The last row reports the results obtained using jointly all the data with the exception of Experiment 4.

Experiment	N	$\hat{\lambda}$	$\hat{\beta}$	$\hat{\sigma}_\lambda$	$\hat{\sigma}_\beta$	m_{inf}	S_o^{inf}	k_{ro}^{inf}	$\hat{\sigma}_k^2$
1	14	17.78	32.93	2.37	4.75	4.70	0.33	0.23	3.50×10^{-5}
2	8	13.17	22.55	0.70	1.34	3.70	0.38	0.27	4.73×10^{-6}
3	11	36.87	76.08	3.30	7.72	8.93	0.28	0.18	1.38×10^{-6}
4	7	15.85	22.81	0.82	1.30	4.28	0.47	0.33	6.22×10^{-6}
5	11	18.28	34.06	3.41	7.92	4.82	0.33	0.22	9.21×10^{-7}
6	14	17.89	31.47	4.40	8.36	4.73	0.36	0.24	1.31×10^{-6}
Joint	58	13.26	22.37	1.54	2.97	3.73	0.38	0.27	1.12×10^{-4}

Fig. 7 reports the observed and predicted three-phase oil permeabilities versus oil saturation for each experiment. The figure juxtaposes predictions obtained with model parameters estimated solely via two-phase data (dashed curves) and those obtained through ML model calibration on three-phase measurements (solid curves). Intervals of width equal to $\pm\hat{\sigma}_k$ and centered around ML-based model results are also shown. In general, the experimental data lie within the uncertainty bounds of width $\pm\hat{\sigma}_k$. A significant difference between model predictions based on two-phase data and those obtained relying on three-phase information is observed for Experiment 4 (as expected following the considerations illustrated above) and Experiment 3. In this latter case we observe that the two prediction curves are nearly indistinguishable within the saturation range where the experimental data are available (i.e., for $k_{ro}^{G*} < 10^{-2}$).

Fig. 8 compares $(\bar{\lambda}, \bar{\beta})$ against ML estimates $(\hat{\lambda}, \hat{\beta})$. The value of $\bar{\beta}$ is comprised within the interval $[\hat{\beta}-2\hat{\sigma}_\beta, \hat{\beta}+2\hat{\sigma}_\beta]$ for Experiments 1, 5 and 6 and is slightly larger than $\hat{\beta}-2\hat{\sigma}_\beta$ for Experiments 2 and 4, where it can be seen that $\hat{\beta}$ is associated with very narrow uncertainty bounds. The estimate $\bar{\lambda}$ is comprised within the interval $[\hat{\lambda}-2\,\hat{\sigma}_\lambda, \hat{\lambda}+2\hat{\sigma}_\lambda]$ for Experiments 1, 4, 5 and 6, and slightly overestimates $\hat{\lambda}$ for Experiment 2. A notable difference between $\hat{\beta}$ and $\bar{\beta}$ and between $\hat{\lambda}$ and $\bar{\lambda}$ is observed only for Experiment 3. In this case the order of magnitude of all three-phase relative permeability data is smaller or equal to that of $\hat{\sigma}_k$ (i.e., $O(10^{-3})$),

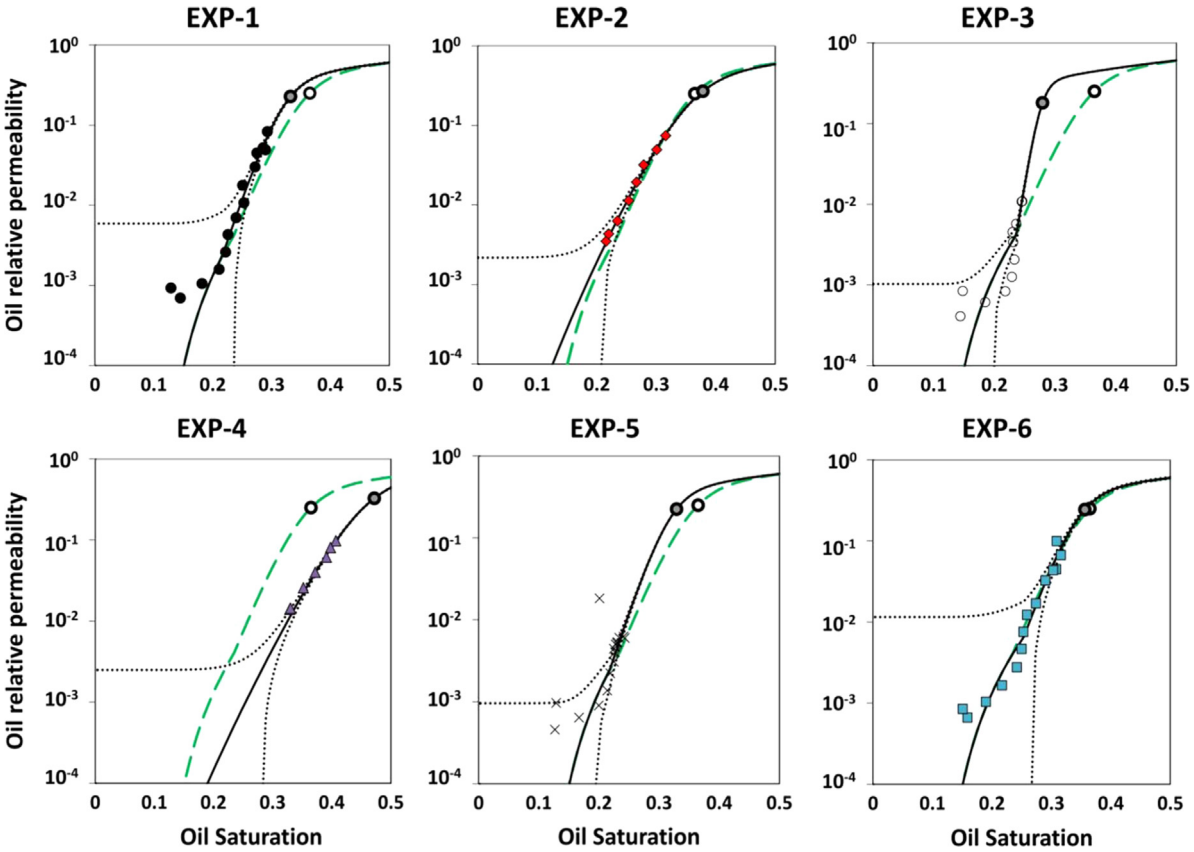

Fig. 7. Predictions of three-phase oil relative permeabilities following primary gas injection based on (1)–(3) and experimental data by Oak (1990) (symbols) versus oil saturation. Green dashed curves are obtained with parameters listed in Table 1. Black solid curves represent model results obtained by ML calibration on three-phase data; dotted curves correspond to intervals of width $\pm\hat{\sigma}_k$ (see Table 2). Empty and gray circles indicate the coordinates of the inflection point of the sigmoid model.

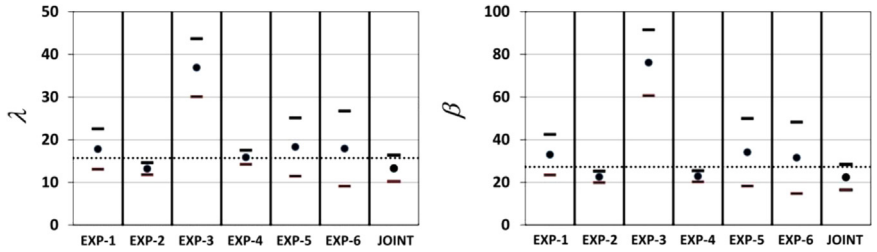

Fig. 8. Maximum likelihood estimates (•) $\hat{\lambda}$ (left), and $\hat{\beta}$ (right). Horizontal dashed lines represent the values calculated for $\overline{\lambda}$ (left) and $\overline{\beta}$ (right) using solely the available two-phase data. The width of the vertical intervals centered at ML parameter estimates (▪) is equal to $\pm 2\hat{\sigma}_{\lambda}$ (left) and $\pm 2\hat{\sigma}_{\beta}$ (right).

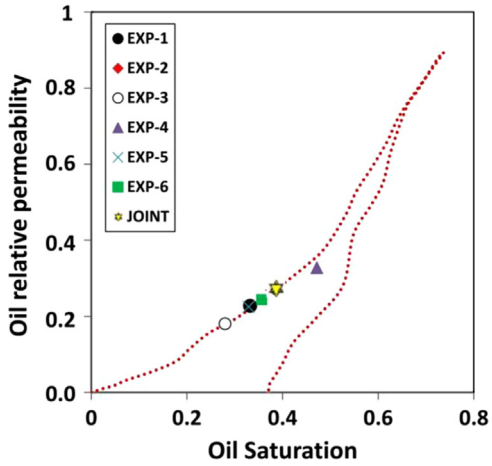

Fig. 9. Juxtaposition of the position of the inflection points calculated according to ML estimates $\hat{\lambda}$ and $\hat{\beta}$ and the two-phase oil relative permeability curves provided by Oak (1990) in an oil–water system (dashed curves).

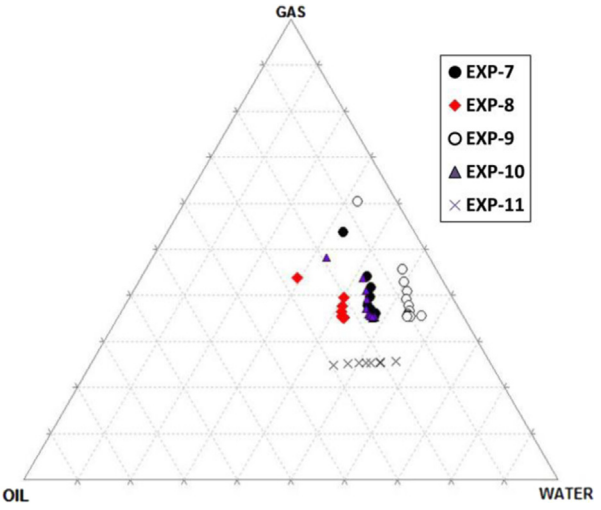

Fig. 10. Saturation paths of the secondary water injection experiments considered. Data are from Oak (1990).

as seen in Table 2 and Fig. 7). We further note that according to (2) the predicted values of k_{ro}^{G} coincide with $\overline{k}_{rog}$ in this case. As a consequence, the large parameters variations observed in Fig. 8 have no influence on the model performance for Experiment 3 and the calibrated and predicted relative permeabilities are in agreement for most of the data, as also seen in Fig. 7.

When the data of all experiments (with the exclusion of Experiment 4) are jointly considered, it can be seen that the uncertainty associated with $(\hat{\lambda}, \hat{\beta})$ generally decreases. Nonetheless, both $\overline{\lambda}$ and $\overline{\beta}$ fall within the bounds of uncertainty associated with ML calibrations, as depicted in Fig. 8.

Finally, Fig. 9 juxtaposes the ML calibrated inflection point positions (evaluated for each experiment and considering jointly all the experiments; see also Table 2) and the oil relative permeability curves observed in a two-phase oil–water system. It can be seen that ML estimates $\hat{\lambda}$ and $\hat{\beta}$ lead to values of $(S_o^{inf}, k_{ro}^{inf})$ which lie on the drainage relative permeability curve for a two-phase oil–water system. This results supports our working hypothesis introduced in Section 3.1.1 according to which estimates of three-phase oil permeability can be obtained only on the basis of two-phase data.

4.1.2. Secondary water injection

We consider a set of five secondary water injection experiments performed by Oak (1990). The saturation paths of the five experiments are depicted in Fig. 10. The three-phase relative permeability, k_{ro}^{W}, is modeled through (5).

The characteristics of the inflection point obtained by (3)–(4) together with estimates $(\overline{\lambda}_{ow}, \overline{\beta}_{ow})$ of $(\lambda_{ow}, \beta_{ow})$ obtained by using only two-phase data according to the procedure illustrated in Section 3.1.2 are listed in Table 3. Fig. 11a depicts the scatterplot of

Table 3
Estimates $(\overline{\lambda}_{ow}, \overline{\beta}_{ow})$, coordinates $(S_{ow}^{inf}, k_{row}^{inf})$ of the inflection point and m_{ow}^{inf} derived from secondary water injection experiments reported by Oak (1990).

$\overline{\lambda}_{ow}$	$\overline{\beta}_{ow}$	S_{ow}^{inf}	k_{row}^{inf}	m_{ow}^{inf}
6.36	8.91	0.55	0.42	2.26

predicted and observed three-phase oil permeability values associated with these experimental conditions. Almost all experimental data are reproduced with a satisfactory accuracy. These results suggest that our sigmoid-based model can effectively interpret the relationship between relative permeability and saturation in water-wet media under secondary water injection.

Maximum likelihood estimates of model parameters based on three-phase data are reported in Table 4 together with the corresponding estimated standard deviation, $\hat{\sigma}_{\lambda_{ow}}$ and $\hat{\sigma}_{\beta_{ow}}$. Note that in this case all experimental data are jointly considered, as the model parameters do not depend on the initial oil saturation. Fig. 11b is the corresponding scatterplot of predicted and observed three-phase oil permeability values. Comparison of Fig. 11a-b suggests that reliance of our model only on two-phase data leads to model predictions whose quality is very similar to that obtained by direct model calibration on three-phase data. Note that the ML estimate $\hat{\beta}_{ow}$ listed in Table 4 is about 25% smaller than the value of $\overline{\beta}_{ow}$ reported in Table 3. This difference might be due to the observations that (i) notable changes in the position of the sigmoid model inflection point induce small variations of k_{row}^{S} for low oil saturation values, and/or (ii) k_{ro}^{W} is the saturation-weighted interpolation of the sigmoid function k_{row}^{S} and $\overline{k}_{rog}$, the latter being independent of model parameters, so that the final predicted relative permeability is not very sensitive to parameter variations of the kind reported above.

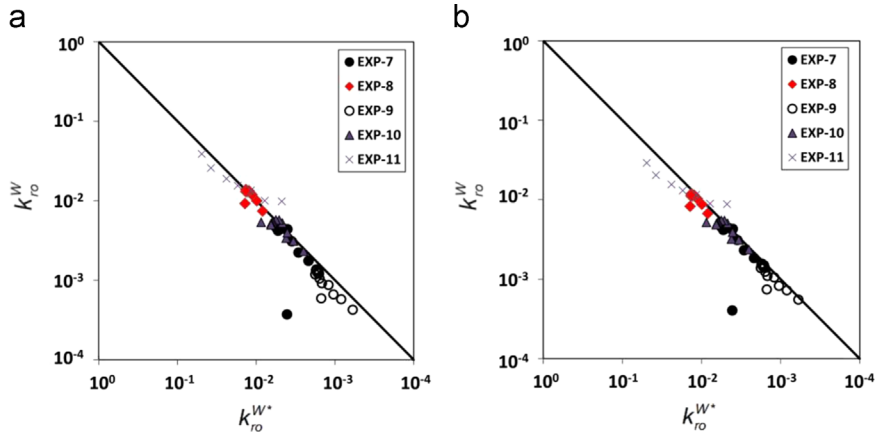

Fig. 11. Scatterplot of observed (k_{ro}^{W*}) and predicted (k_{ro}^{W}) three-phase oil relative permeability values. Data are associated with secondary water injection experiments performed by Oak (1990). Model results are obtained through (a) parameter estimates based solely on two-phase data (see Table 3); and (b) ML calibrated model parameters (see Table 4).

Table 4
Number of available three-phase relative permeability data (N), ML estimates ($\hat{\lambda}_{ow}, \hat{\beta}_{ow}$) and corresponding estimation error standard deviations, k_{ro}^{inf}, coordinates (S_{ow}^{inf}, k_{row}^{inf}) of the inflection point of (5) and ML estimate $\hat{\sigma}_k^2$ of the variance of three-phase oil permeability measurement errors derived from secondary water injection experiments reported by Oak (1990).

N	$\hat{\lambda}_{ow}$	$\hat{\beta}_{ow}$	$\hat{\sigma}_{\lambda_{ow}}$	$\hat{\sigma}_{\beta_{ow}}$	m_{ow}^{inf}	S_{ow}^{inf}	k_{row}^{inf}	$\hat{\sigma}_k^2$
57	5.57	6.98	0.37	0.89	2.11	0.69	0.56	5.66×10^{-6}

4.2. Analysis of the data of DiCarlo et al. (2000)

We consider here a total of 8 datasets presented by DiCarlo et al. (2000) to assess the reliability of our modeling strategy under diverse wettability conditions. These data are representative of oil three-phase relative permeability measurements obtained through gas gravity drainage under water-wet, oil-wet, fractionally-wet, and mixed-wet conditions. Fractionally-wet media are composed by a mixture of water-wet and oil-wet grains. Mixed-wet systems are generated through oil-flooding and aging of an initially water-wet medium. This induces a wettability change on the solid surfaces which are in contact with oil. As a result, large pores tend to become oil-wet whereas small pores and throats tend to remain water-wet. All experiments start from two-phase (oil–water) initial condition and consider drainage flow of gas.

We note that while the Oak (1990) experiments analyzed in Section 4.1 were performed under forced injection of water or gas, the DiCarlo et al. datasets are associated with dynamic displacements (of gas/water/oil) driven by gravity. Two-phase water–oil data are not available in this case. Therefore, only the ML parameter calibration strategy described in Section 3.2 is applied. According to DiCarlo et al. (2000), we set $\overline{k}_{row}^{M} = 0.2$ and $\overline{S}_{ow}^{M} = 0.8$, 0.95, 0.85 and 0.9, respectively for water-wet, oil-wet, fractionally-wet, and mixed-wet conditions.

The following two different initial conditions were employed during the experiments:

(i) initial water saturation coinciding with connate water saturation, $\overline{S}_{wc}$, (Experiments 1–4); note that in this case the oil relative permeability measured during the gas drainage corresponds to $\overline{k}_{rog}$;
(ii) initial oil saturation coinciding with residual oil saturation, $\overline{S}_{row}$ (Experiments 5–8).

The wettability conditions associated with each experiment are listed in Table 5. On these bases, data analysis is performed through the following steps:

(i) we describe $\overline{k}_{rog}$ through a sigmoid-based model whose parameters are estimated through a ML procedure (see Section 3.2) and by making use of the oil relative permeability data observed in Experiments 1–4;
(ii) k_{ro}^{G} is estimated through (2) using $\overline{k}_{rog}$ determined at step (a) and the ML estimates of the parameters of the sigmoid curve k_{ro}^{GS} obtained using the outcomes of Experiments 5–8.

Results of the calibration procedure are listed in Table 5 for each experiment. Fig. 12 is a scatterplot of predicted and observed three-phase oil relative permeability values. ML estimates $\hat{\lambda}$ do not vary significantly across the experiments analyzed, and nearly coincide for Experiments 1–4. On the other hand, $\hat{\beta}$ varies significantly across the experiments. This finding suggests that wettability effects might be embedded in β.

To further explore this issue, Fig. 13 depicts the sigmoid model results obtained on the basis of the calibrated parameters listed in Table 5. Consistent with the results of the sensitivity analysis illustrated in Fig. 1, variations of $\hat{\beta}$ affect the trend of the relative permeability curves only at low oil saturations, thus supporting the observation that β might indeed incorporate effects associated with diverse wettability conditions.

This hypothesis is also supported by the observation that the value of $\hat{\beta}$ listed in Table 5 for the water-wet system ($\hat{\beta}=22.95$, Experiment 5) is very close to the one obtained from the Oak dataset ($=22.37$, see Table 2) for the same wettability conditions and considering jointly all the data.

Fig. 13b reveals that the three-phase oil relative permeability at low saturations (< 0.1) is largest for water-wet and smallest for oil-wet systems. Fractionally- and mixed-wet conditions are associated with intermediate values of k_{ro}^{G}. The slope of the sigmoid curve at the inflection point, m_{inf}, is of the order of 0.6 (see Table 5). This value is significantly smaller than the one observed for the Oak dataset (see Table 2). This difference may be related to a reduced rate of change of relative permeability associated with gas gravity drainage in a sand pack with respect to what can be observed in the steady state injection for a consolidated sandstone in Oak (1990). This effect seems to be embodied in the parameter λ (compare the values of $\hat{\lambda}$ in Table 5 for Experiment 5 and in Table 2, last row). As such, λ may potentially include the macroscale effect of key displacement mechanisms taking place at the pore scale.

Table 5

Number of available three-phase relative permeability data (N), ML estimates ($\hat{\lambda}, \hat{\beta}$) and corresponding estimation error standard deviations, m_{inf}, coordinates (S_o^{inf}, k_{ro}^{inf}) of the inflection point of (5) and ML estimate of the variance $\hat{\sigma}_k^2$ of three-phase oil permeability measurement errors derived from experiments reported by DiCarlo et al. (2000).

Initial condition	Experiment	N	$\hat{\lambda}$	$\hat{\beta}$	$\hat{\sigma}_\lambda$	$\hat{\sigma}_\beta$	m_{inf}	S_o^{inf}	k_{ro}^{inf}	$\hat{\sigma}_k^2$
$\overline{S}_{wc}$	1 (water-wet)	91	8.42	14.14	0.85	1.27	0.59	0.46	0.07	3.65×10^{-5}
	2 (oil-wet)	73	8.61	16.89	3.24	5.63	0.57	0.50	0.06	3.34×10^{-4}
	3 (fractionally-wet)	33	8.94	14.12	4.02	6.07	0.62	0.46	0.08	8.89×10^{-4}
	4 (mixed-wet)	74	8.72	24.99	3.02	8.56	0.58	0.30	0.04	9.12×10^{-6}
$\overline{S}_{row}$	5 (water-wet)	69	8.46	22.95	0.89	3.95	0.60	0.25	0.04	8.16×10^{-8}
	6 (oil-wet)	72	9.69	24.84	0.70	3.58	0.61	0.37	0.05	2.57×10^{-9}
	7 (fractionally-wet)	60	9.62	18.47	1.23	4.19	0.66	0.35	0.06	2.59×10^{-8}
	8 (mixed-wet)	75	10.10	31.33	1.12	5.65	0.64	0.27	0.04	2.79×10^{-8}

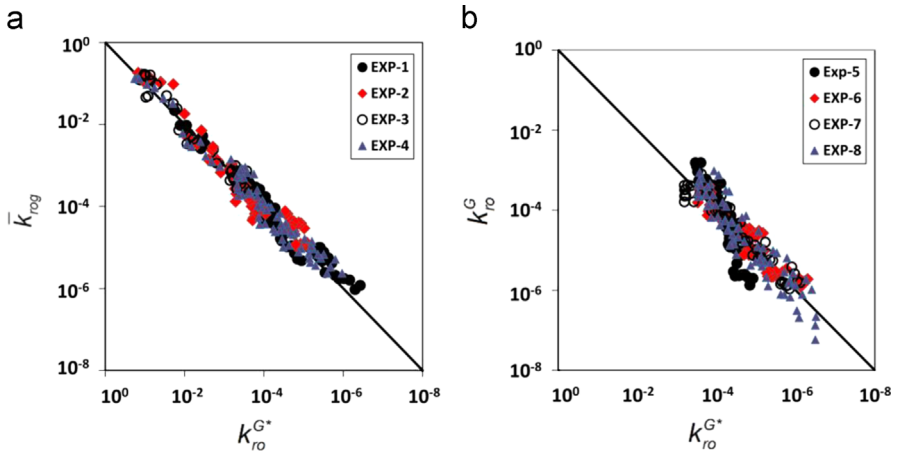

Fig. 12. Scatterplot of predicted oil relative permeabilities versus experimental data from DiCarlo et al. (2000). The results are associated with experiments starting from (a) $\overline{S}_{wc}$ or (b) $\overline{S}_{row}$ as initial condition. Model results are obtained through the parameters reported in Table 5.

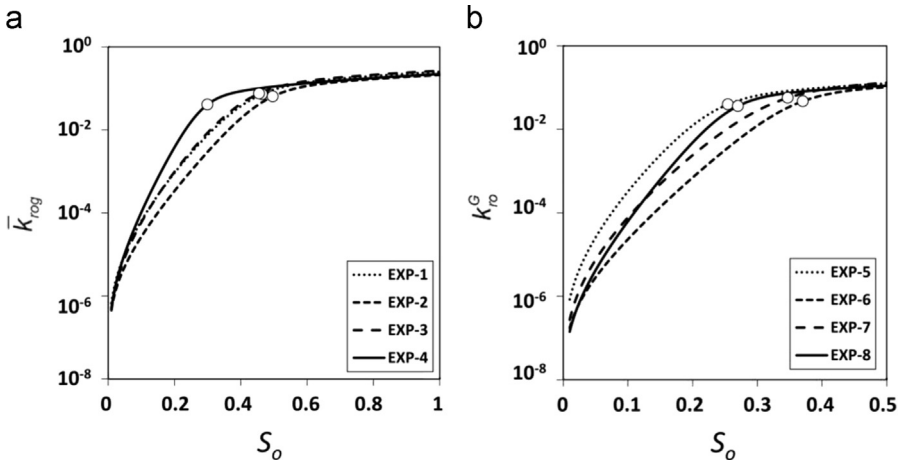

Fig. 13. Results associated with experiments of DiCarlo et al. (2000) and obtained by employing (a) $\overline{S}_{wc}$ or (b) $\overline{S}_{row}$ as the model initial condition. Model results are based on parameters listed in Table 5. Empty circles indicate the position of the inflection points.

The soundness of these observations should be further tested by performing and analyzing additional three-phase oil relative permeability data obtained under diverse wettability and flow conditions.

5. Concluding remarks

We have introduced a new empirical model to predict three-phase oil relative permeabilities during primary gas injection and secondary water injection. Since three-phase data are rarely available, we also propose a methodology to estimate all model parameters upon relying solely on two-phase data. Displacement mechanisms considered are gas gravity drainage and continuous steady-state injection of the three phases.

Our model is based on a sigmoid functional format. This mathematical representation is selected because it can represent variations of the concavity in the oil saturation–relative permeability relationship caused by oil remobilization and layer drainage regime.

We start from the hypothesis that three-phase oil relative permeabilities for primary gas injection can be predicted through our proposed sigmoid curve. The inflection point of the sigmoid model lies on the drainage oil saturation–relative permeability

curve of a two-phase oil–water system. The slope of the sigmoid at the inflection point is set to the maximum slope of the oil relative permeability–saturation curve in an oil–gas system with connate water. We then estimate the relative permeability associated with secondary water injection by means of saturation-weighted interpolation and a sigmoid function representing the oil relative permeability in a two-phase oil–water system. The results obtained through this working hypothesis are compared against two sets of experimental data. The comparisons show that most experimental observations are accurately reproduced by the proposed models, which can also include wettability effects. We also performed a Maximum Likelihood calibration of the model parameters against direct measurements of three-phase relative permeabilities, supporting the robustness of the proposed approach.

Acknowledgments

We acknowledge Prof. David DiCarlo for sharing with us the experimental data. E.R., G.P., A.G. and M.R. are grateful for the partial financial support from Eni SpA.

References

Alizadeh, A.H., Piri, M., 2014. Three-phase flow in porous media: a review of experimental studies on relative permeability. Rev. Geophys. 52, 468–521 http://dx.doi.org/10.1002/2013RG000433.

Alizadeh, A.H., Piri, M., 2013. The effect of saturation history on three-phase relative permeability: an experimental study, SCA2013-023. In: Proceedings of International Symposium of the Society of Core Analysts, California, USA, September 16–19.

Atashpaz-Gargari, E., Lucas, C., 2007. Imperialist competitive algorithm: an algorithm for optimization inspired by imperialistic competition. In: Proceedings of the 7th IEEE Congress on Evolutionary Computation, Singapore, September 25–27.

Aziz, K., Settari, A., 1979. Petroleum Reservoir Simulation. Applied Science Publishers, London.

Baker, L.E., 1988. Three phase relative permeability correlation, SPE/DOE 17369. In: Proceedings of the SPE/DOE Symposium on Enhanced Oil Recovery, Tulsa, USA, April 17–20, http://dx.doi.org/10.2118/17369-MS.

Blunt, M.J., 2000. An empirical model for three-phase relative permeability. SPE J. 5, 435–445. http://dx.doi.org/10.2118/67950-PA.

Carlson, F.M., 1981. Simulation of relative permeability hysteresis to the nonwetting phase, SPE 10157. In: Proceedings of the SPE Annual Technical Conference and Exhibition, San Antonio, Texas, October 5–7, http://dx.doi.org/10.2118/10157-MS.

Carrera, J., Neuman, S.P., 1986. Estimation of aquifer parameters under transient and steady state conditions: 1. Maximum likelihood method incorporating prior information. Water Resour. Res. 22 (2), 199–210. http://dx.doi.org/10.1029/WR022i002p00199.

Corey, A.T., Rathjens, C.H., 1956. Effect of stratification on relative permeability. J. Petrol. Technol. 8, 69–71. http://dx.doi.org/10.2118/744-G.

Delshad, M., Pope, G.A., 1989. Comparison of the three-phase oil relative permeability models. Transp. Porous Media 4, 59–83. http://dx.doi.org/10.1007/BF00134742.

DiCarlo, D.A., Sahni, A., Blunt, M.J., 2000. The effect of wettability on three-phase relative permeability. Transp. Porous Media 39, 347–366. http://dx.doi.org/10.1023/A:1006653323374.

Doherty, J., 2005. Model-independent parameter estimation, PEST User Manual: 5th Edition.

Egermann, P., Vizika, O., Dallet, L., Requin, C., Sonier, F., 2000. Hysteresis in Three-Phase Flow: Experiments, Modeling and Reservoir Simulations, SPE 65127, Presented in SPE European Petroleum Conference, Paris, France, October 24–25, http://dx.doi.org/10.2118/65127-MS.

Fenwick, D.H., Blunt, M.J., 1998. Network modeling of three-phase flow in porous media. SPE J. 3, 86–97. http://dx.doi.org/10.2118/38881-PA.

Jerauld, G.R., 1997. General three-phase relative permeability model for Prudhoe Bay. SPE Reserv. Eng. 12, 255–263. http://dx.doi.org/10.2118/36178-PA.

Killough, J.E., 1976. Reservoir simulation with history-dependent saturation functions. SPEJ, Trans., AIME 261, 37–48. http://dx.doi.org/10.2118/5106-PA.

Land, C.S., 1968. Calculation of imbibition relative permeability for two- and three-phase flow from rock properties. SPEJ, Trans., AIME 243, 149–156. http://dx.doi.org/10.2118/1942-PA.

Larsen, J.A., Skauge, A., 1998. Methodology for numerical simulation with cycle-dependent relative permeabilities. SPE J. 3, 163–173. http://dx.doi.org/10.2118/38456-PA.

Mani, V., Mohanty, K.K., 1997. Effect of the spreading coefficient on three-phase flow in porous media. J. Colloid Interface Sci. 187, 45–56. http://dx.doi.org/10.1006/jcis.1996.4700.

Medina, A., Carrera, J., 2003. Geostatistical inversion of coupled problems: dealing with computational burden and different types of data. J. Hydrol. 281, 251–264. http://dx.doi.org/10.1016/S0022-1694(03)00190-2.

Nocedal, J., Wright, S.J., 2006. Numerical Optimization, second ed. Springer, New York.

Oak, M.J., 1990. Three-phase relative permeability of water-wet Berea, SPE 20183. In: Proceedings of the 7th SPE/DOE Enhanced Oil Recovery Symposium, Tulsa, Oklahoma, April 22–25, http://dx.doi.org/10.2118/20183-MS.

Oak, M.J., Baker, L.E., Thomas, D.C., 1990. Three-phase relative permeability of Berea sandstone. J. Petrol. Technol. 42, 1054–1061. http://dx.doi.org/10.2118/17370-PA.

Oliveira, L.I., Demond, A.H., 2003. Estimation of primary drainage three-phase relative permeability for organic liquid transport in the vadose zone. J. Contam. Hydrol. 66, 261–285. http://dx.doi.org/10.1016/S0169-7722(03)00029-9.

Piri, M., Blunt, M.J., 2005. Three-dimensional mixed-wet random pore-scale network modeling of two and three-phase flow in porous media, I. Model description. Phys. Rev. E 71, 206–301. http://dx.doi.org/10.1103/PhysRevE.71.026301.

Ranaee, E., Porta, G., Riva, M., Guadagnini, A., 2014. Investigation of saturation dependency of oil relative permeability during WAG process through linear and non-linear PCA. In: Proceeding of ECMOR XIV-14th European Conference on the Mathematics of Oil Recovery, Catania, Italy, September 8–11, http://dx.doi.org/10.3997/2214-4609.20141800.

Riva, M., Guadagnini, A., Neuman, S.P., Bianchi Janetti, E., Malama, B., 2009. Inverse analysis of stochastic moment equations for transient flow in randomly heterogeneous media. Adv. Water Resour. 10, 271–280. http://dx.doi.org/10.1016/j.advwatres.2009.07.003.

Riva, M., Panzeri, M., Guadagnini, A., Neuman, S.P., 2011. Role of model selection criteria in geostatistical inverse estimation of statistical data- and model-parameters. Water Resour. Res. 47, W07502. http://dx.doi.org/10.1029/2011WR010480.

Shahverdi, H., Sohrabi, M., 2012. Three phase relative permeability and hysteresis model for simulation of water alternating gas injection, SPE 152218. In: Proceedings of the 18th SPE Improved Oil Recovery Symposium, Tulsa, Oklahoma, April 14–18, http://dx.doi.org/10.2118/152218-MS.

Sohrabi, M., Danesh, A., Jamiolahmady, M., 2008. Visualisation of residual oil recovery by near-miscible gas and SWAG injection using high-pressure micro-models. Transp. Porous Media 74, 239–257. http://dx.doi.org/10.1007/s11242-007-9193-5.

Spiteri, E.J., Juanes, R., 2006. Impact of relative permeability hysteresis on the numerical simulation of WAG injection. J. Petrol. Sci. Eng. 50, 115–139. http://dx.doi.org/10.1016/j.petrol.2005.09.004.

Stone, H.L., 1970. Probability model for estimation of three-phase relative permeability. J. Petrol. Technol. 22, 214–218. http://dx.doi.org/10.2118/2116-PA.

Stone, H.L., 1973. Estimation of three-phase relative permeability and residual oil data. J. Can. Petrol. Technol. 12, 53–61. http://dx.doi.org/10.2118/73-04-06.

Suicmez, V.S., Piri, M., Blunt, M.J., 2007. Pore-scale simulation of water alternate gas injection. Transp. Porous Media 66, 259–286. http://dx.doi.org/10.1007/s11242-006-0017-9.

Suicmez, V.S., Piri, M., Blunt, M.J., 2008. Effects of wettability and pore-level displacement on hydrocarbon trapping. Adv. Water Resour. 31, 503–512. http://dx.doi.org/10.1016/j.advwatres.2007.11.003.

Van Dijke, M.I.J., Sorbie, K.S., 2003. Pore-scale modelling of three-phase flow in mixed-wet porous media: multiple displacement chains. J. Petrol. Sci. Eng. 39, 201–216. http://dx.doi.org/10.1016/j.jcis.2004.05.021.

Van Dijke, M.I.J., Sorbie, K.S., Sohrabi, M., Danesh, A., 2006. Simulation of WAG floods in an oil-wet micromodel using a 2-D pore-scale network model. J. Petrol. Sci. Eng. 52, 71–86. http://dx.doi.org/10.1016/j.petrol.2006.03.014.

Wetter, M., Wright, J., 2003. Comparison of a generalized pattern search and a genetic algorithm optimization method. In: Proceedings of the 8th International IBPSA Conference Eindhoven, Netherlands, August 11–14, http://dx.doi.org/10.1.1.121.5457.